25 YEARS AFTER THE DISCOVERY: SOME CURRENT TOPICS ON LENSED QSOs

Santander (Spain), 15th-17th December 2004

Gravitational lensing of QSO spectra

Luka Č. Popović
Astronomical Observatory, Belgrade – AvH fellow, AIP, Potsdam
George Chartas
Astronomy and Astrophysics Department, Pennsylvania State University
Collaborators:
E.Mediavilla, C. Abajas, J.A. Munoz (IAC, La Laguna)
P. Jovanovic, D. Ilic (AOB, Belgrade)
A.F. Zakharov (IOP, Moscow)

1. Some reasons: way magnification may be chromatic?
2. A method (Popovic & Chartas 2004)
3. Some examples (Q0957+561,Q1115+080, PG 1413+273)

QSOs (AGN) emit radiation at a range of wavelengths from the radio to the x-ray (gamma-ray)

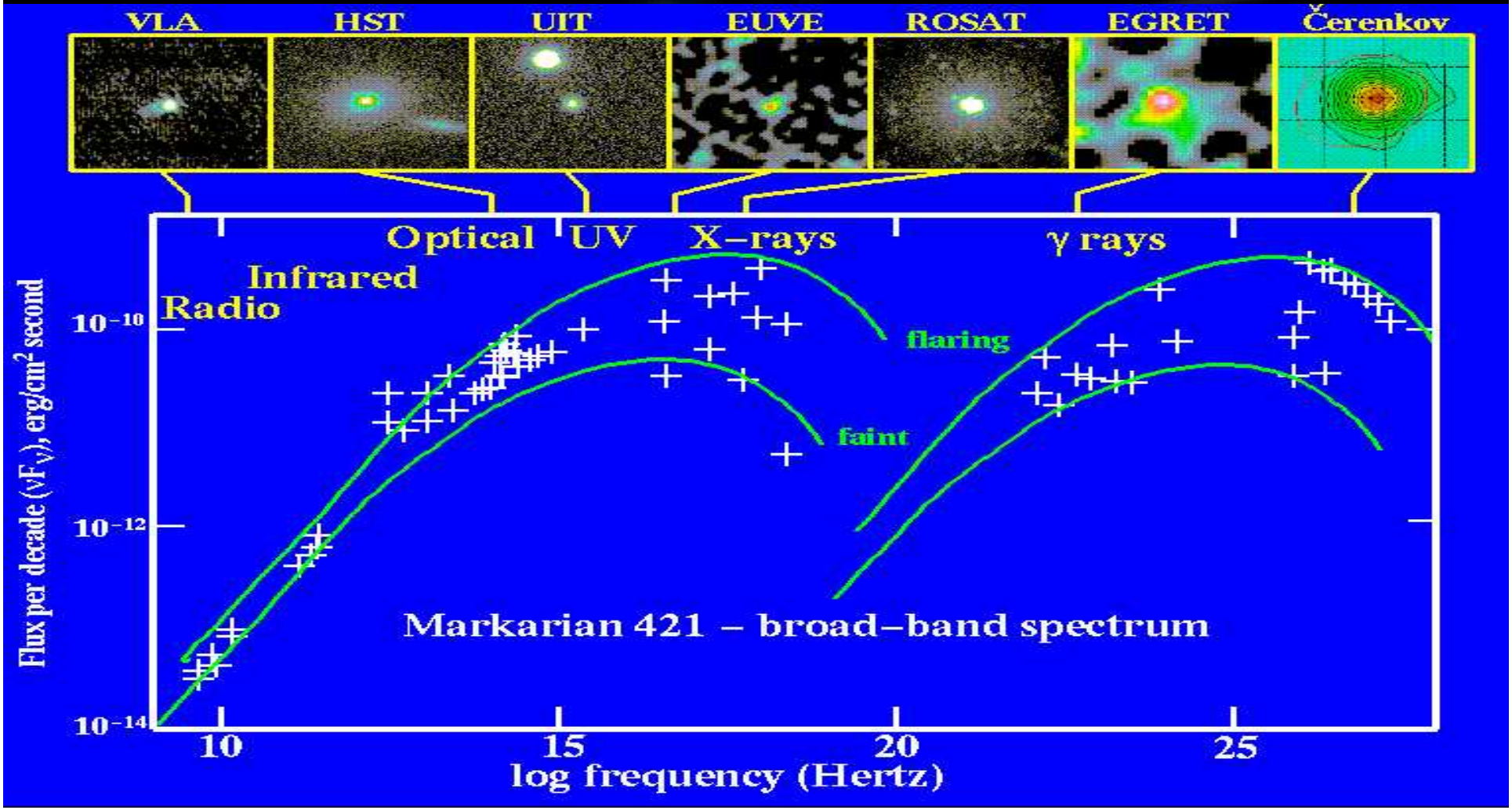

A strong emission of radiation at radio wavelengths

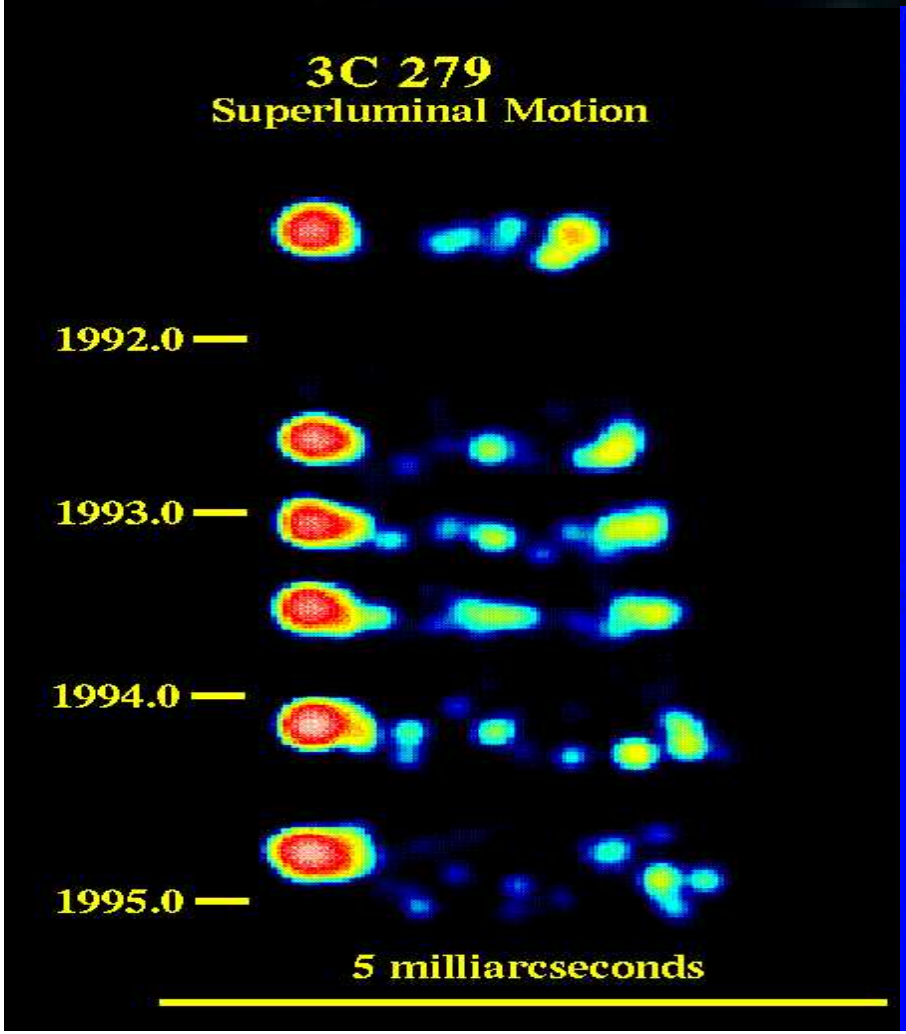

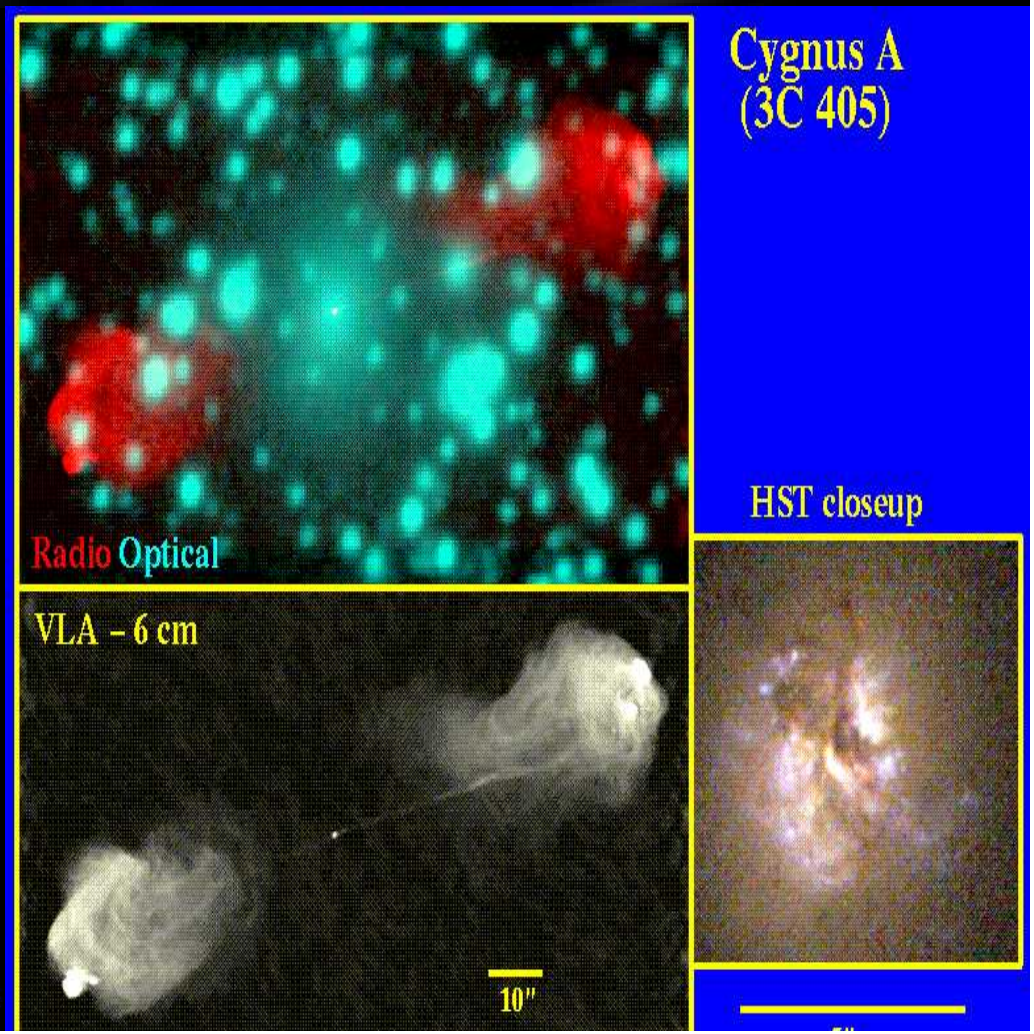

A variability of the continuum and spectral lines (dimensions of emitting regions)

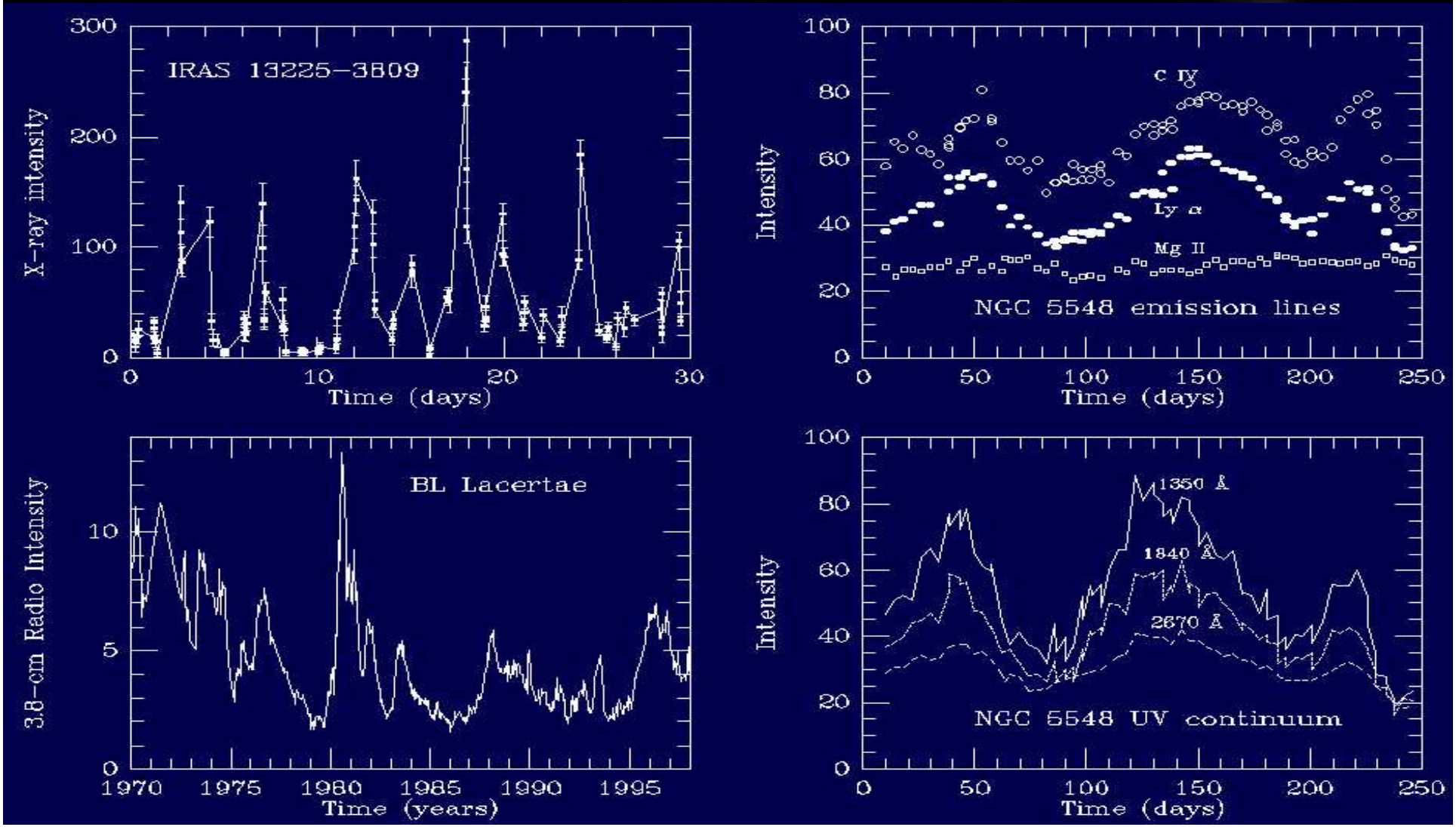

Structure of a QSO - Elvis 2000, ApJ, 545, 63

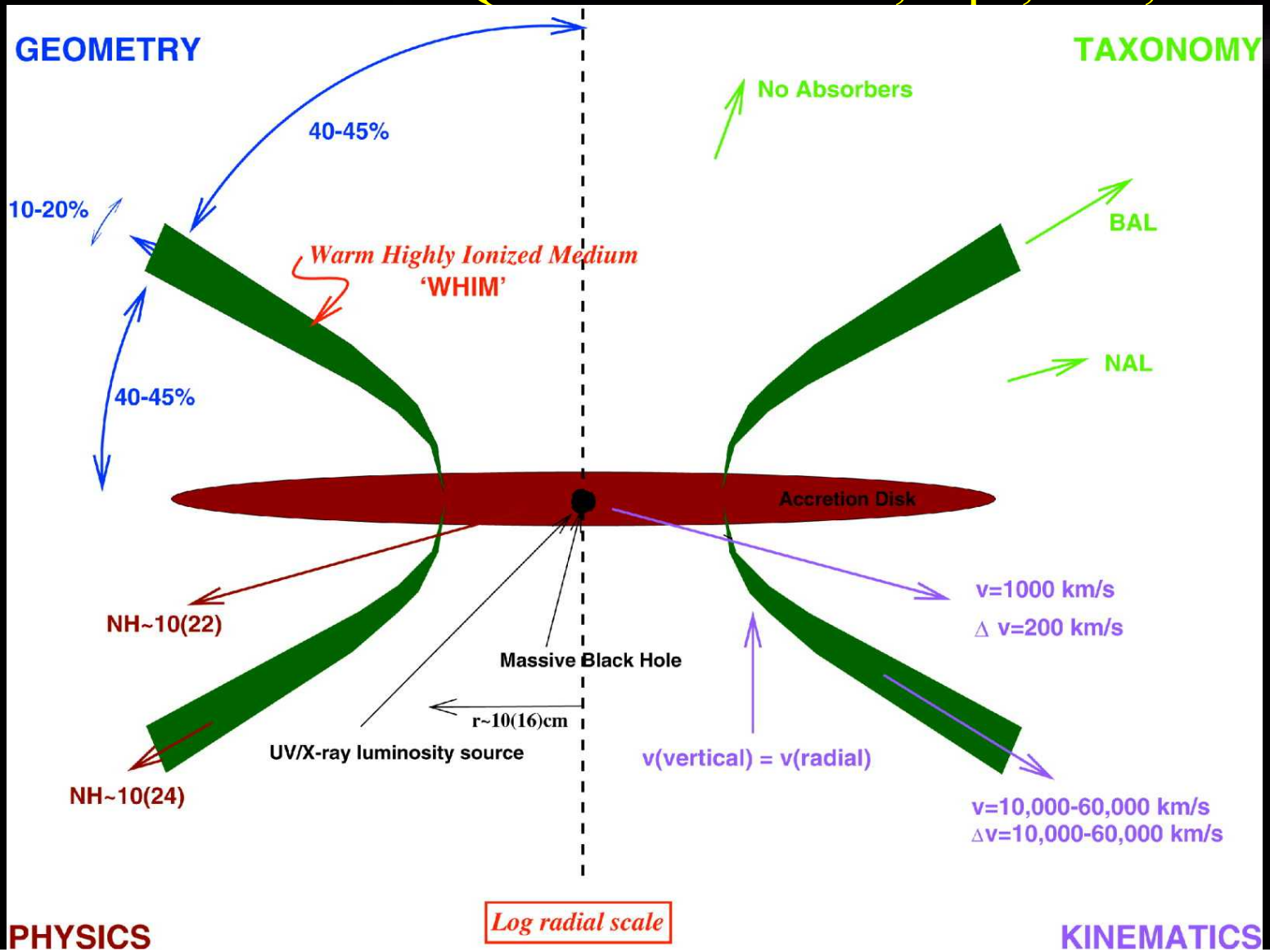

The typical spectra of QSOs in the UV spectral range (Reichard et al. 2003, AJ, 126, 2594)

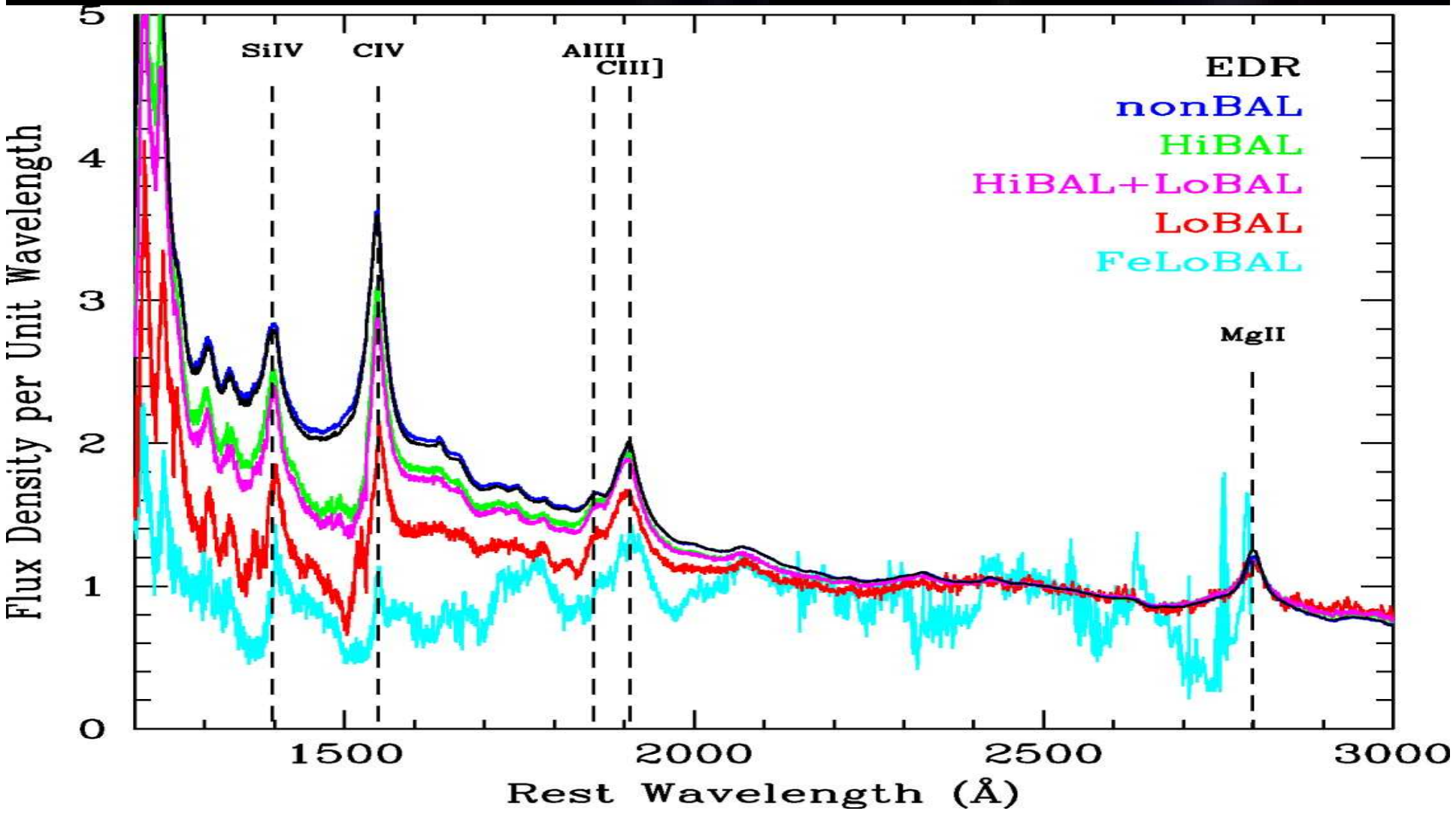

Starting points

1. A lensed QSO has different dimension in different spectral band
2. Kinematics of emitting regions affects the lensed QSO spectra (the continuum and lines)
3. The lens galaxy might have additional gravitational potential (a small galaxy, globular clusters, etc.)
4. ➔ influence of GL on QSO spectra very important for investigations of unresolved QSO central structure

Different dimension of emitting regions:Observations e.g. QSO 2237+0305 : Mediavilla et al. 1998, Metcalf et al. 2004, Motta et al. 2004 (below Fig 2:Map of the integrated flux between 11305.1 and 13613.7 Å (or 4203 to 5061 Å in the QSO's rest frame)); CIII] line and continuum (Motta et al. 2004)

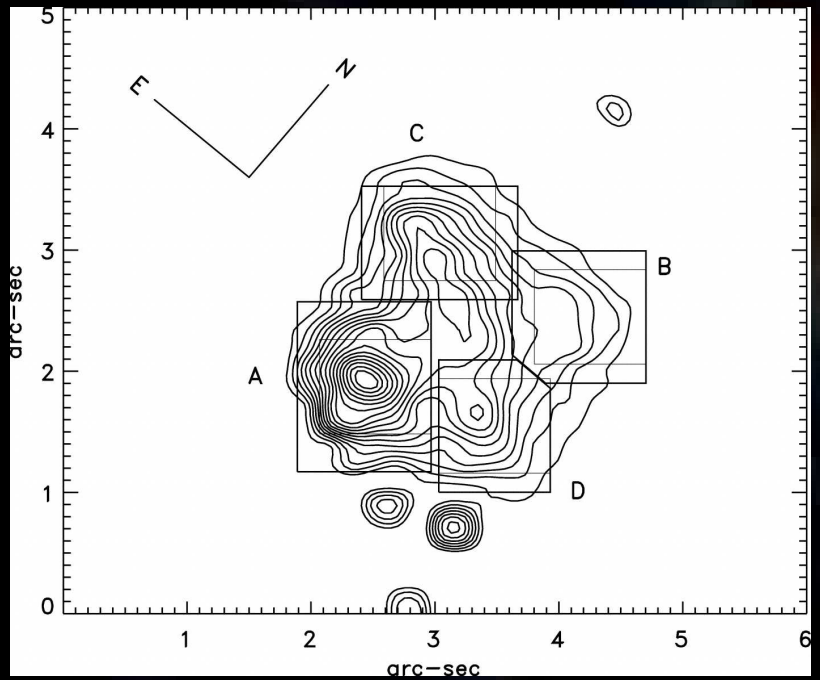

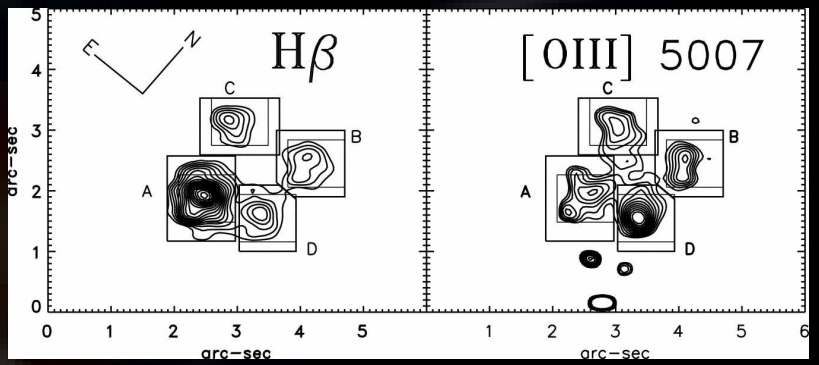

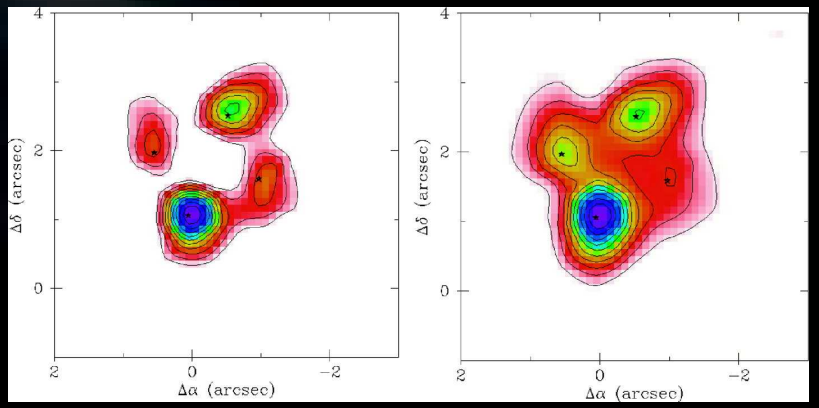

Kinematics of an emission region; e.g. the Fe K-alpha line

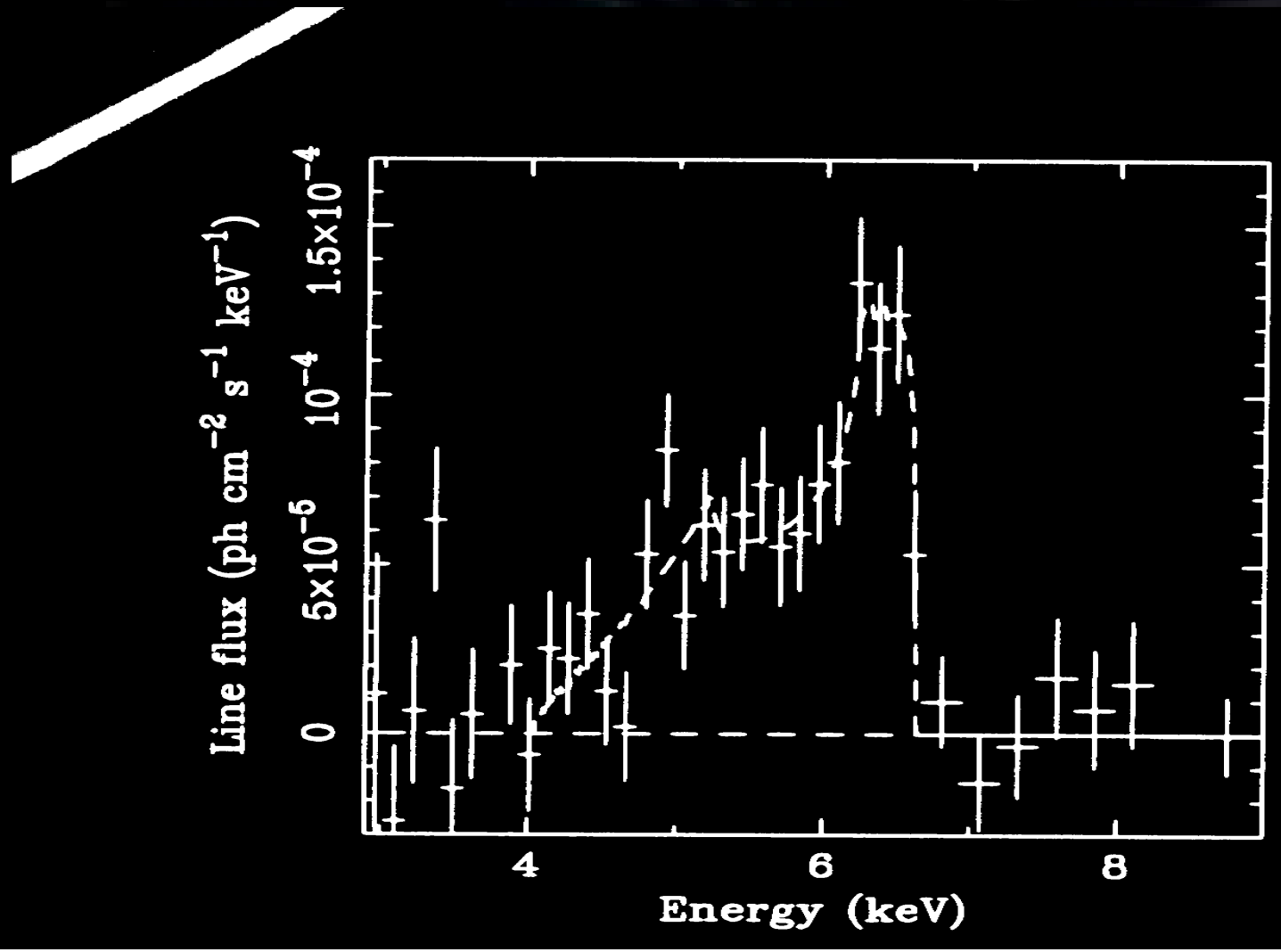

The X-ray accretion disk – Popovic et al. 2003, A&A, 398, 975

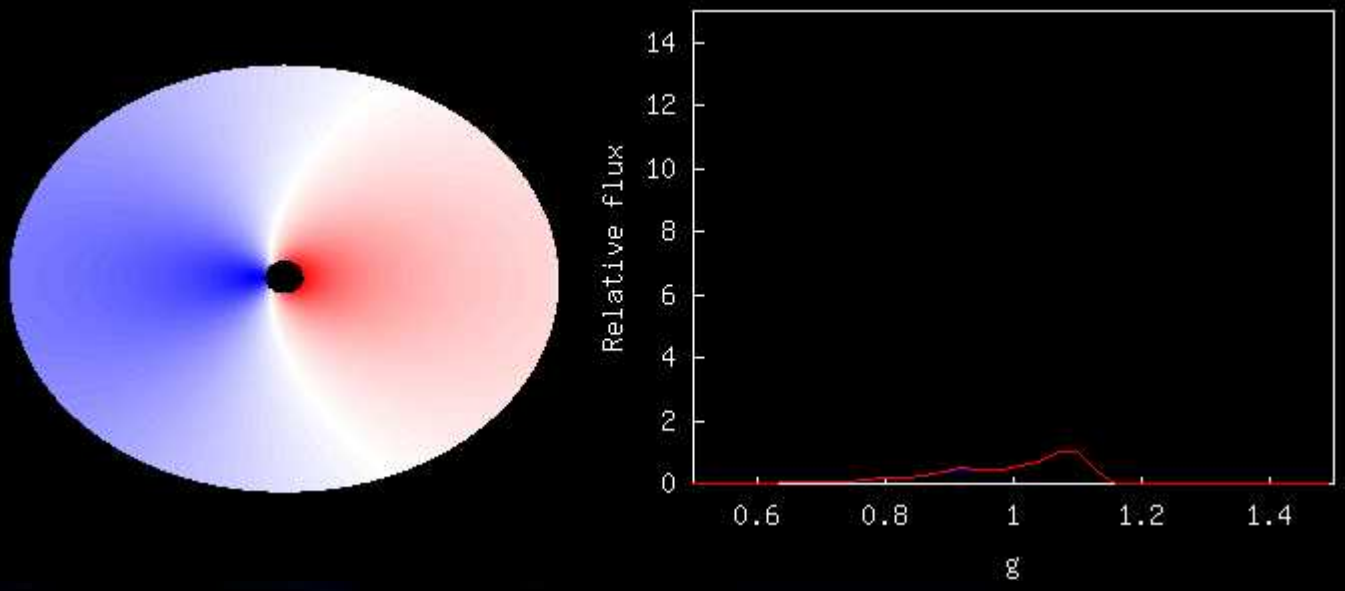

Kerr metric

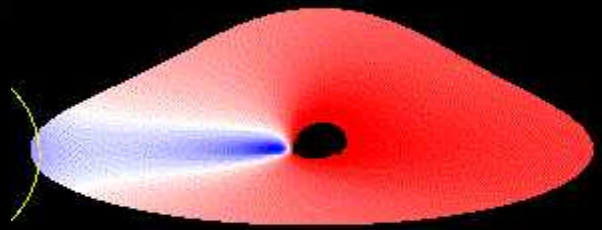

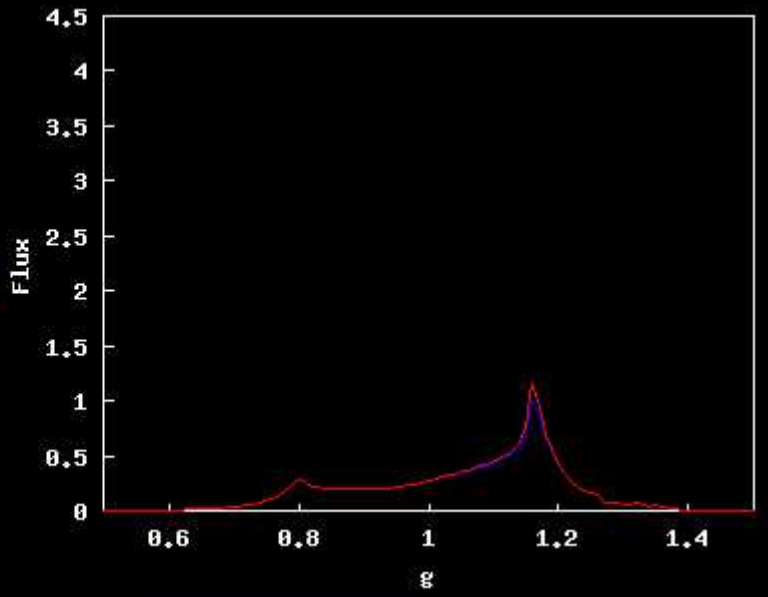

Complex gravitational potential of a lensed galaxy: Mrk 1040

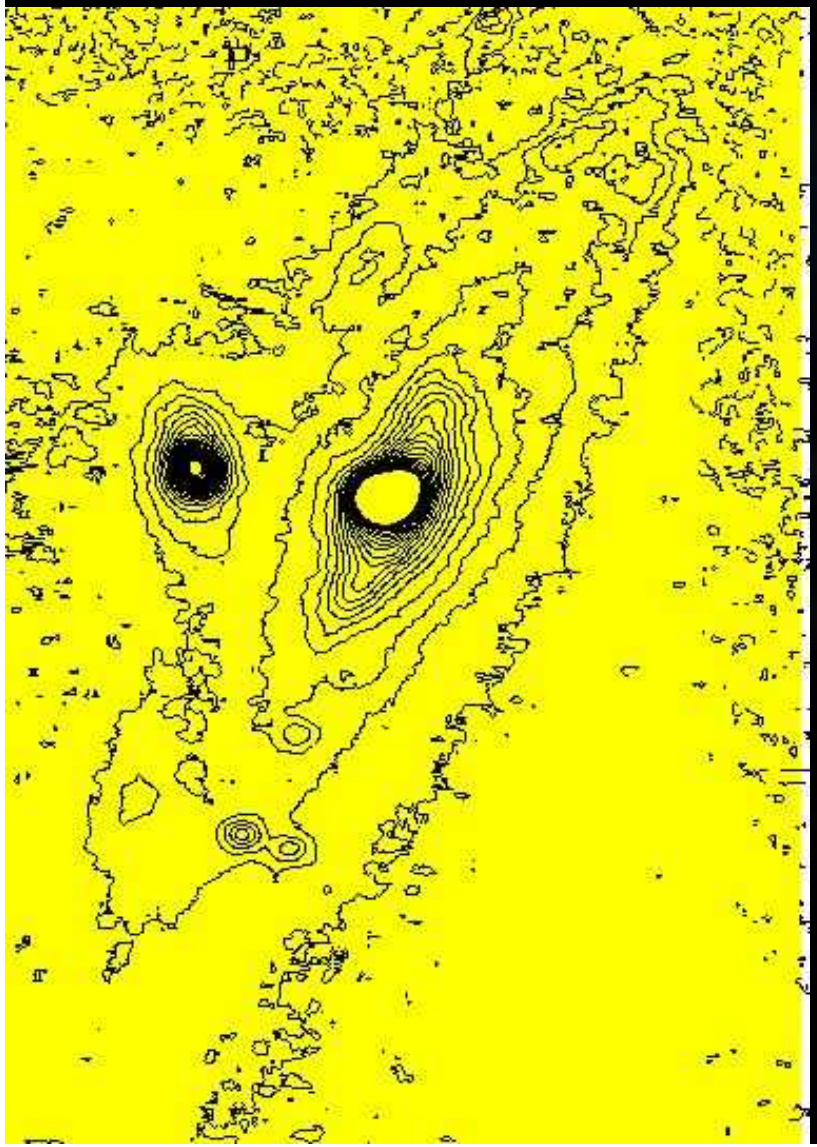

$$I(\lambda; X, Y) = I^c(\lambda; X, Y) + I^L(\lambda; X, Y),$$

where $I^c(\lambda; X, Y)$ and $I^L(\lambda; X, Y)$ are the surface brightnesses of the continuum and the lines, respectively and X,Y are the coordinates of the emission region in the source plane.

$\Im_i(\lambda; X, Y) = \Im_i^c(\lambda; X, Y) + \Im_i^L(\lambda; X, Y)$ where $\Im_i^{c,L}(\lambda; X, Y) = I^{c,L}(\lambda; X, Y) \cdot A(X, Y)$

A(X,Y) might be a complex function and can be represented as function of the X,Y coordinates in the source plane

Microlensing of an image:

$$\Phi_i'(\lambda) = \int_\Sigma \Im_i(\lambda; X, Y) \cdot A_{MLE}(X, Y) d\Sigma = A_i \int_\Sigma [I^c(\lambda; X, Y) + I^L(\lambda; X, Y)] \cdot A_{MLE}(X, Y) d\Sigma$$

where Σ is the projected surface of the macrolensed image at the source distances and A_{MLE} is the amplification due to microlensing.

$$R_{A',A} = \frac{\int_\Sigma [I^c(\lambda; X, Y) + I^L(\lambda; X, Y)] A_{MLE}(X, Y) d\Sigma}{[F^c(\lambda) + F^L(\lambda)]},$$

and the flux ratio between different images observed at the same epoch is

$$R_{A',B'} = \frac{A_1}{A_2} \frac{\int_\Sigma [I^c(\lambda; X, Y) + I^L(\lambda; X, Y)] A_{MLE}(X, Y) d\Sigma}{[F^c(\lambda) + F^L(\lambda)]}.$$

$$\sigma(\lambda) = R_{A',A} - R_{B',B}.$$

$$\overline{A}_{MLE}(\lambda) = \frac{\int_\Sigma [I^c(\lambda; X, Y) + I^L(\lambda; X, Y)] A_{MLE}(X, Y) d\Sigma}{[F^c(\lambda) + F^L(\lambda)]}.$$

From Eqs. (5-7) we write the average magnification caused by microlensing as

$$\overline{A}_{MLE}(\lambda) = \frac{\Phi_A'(\lambda)}{\Phi_A(\lambda)} = \frac{A_2}{A_1} \cdot \frac{\Phi_A'(\lambda)}{\Phi_B'(\lambda)}$$

$$\sigma_I = R_{A',A} - \frac{A_2}{A_1} R_{A',B'} \neq 0$$

$$\overline{A}^L_{MLE}(\lambda) = \frac{\Phi_{A'}(\lambda) - \Phi^c_{A'}(\lambda)}{\Phi_A(\lambda) - \Phi^c_A(\lambda)} == \frac{A_2}{A_1} \frac{\Phi_{A'}(\lambda) - \Phi^c_{A'}(\lambda)}{\Phi_{B'}(\lambda) - \Phi^c_{B'}(\lambda)}$$

LINES

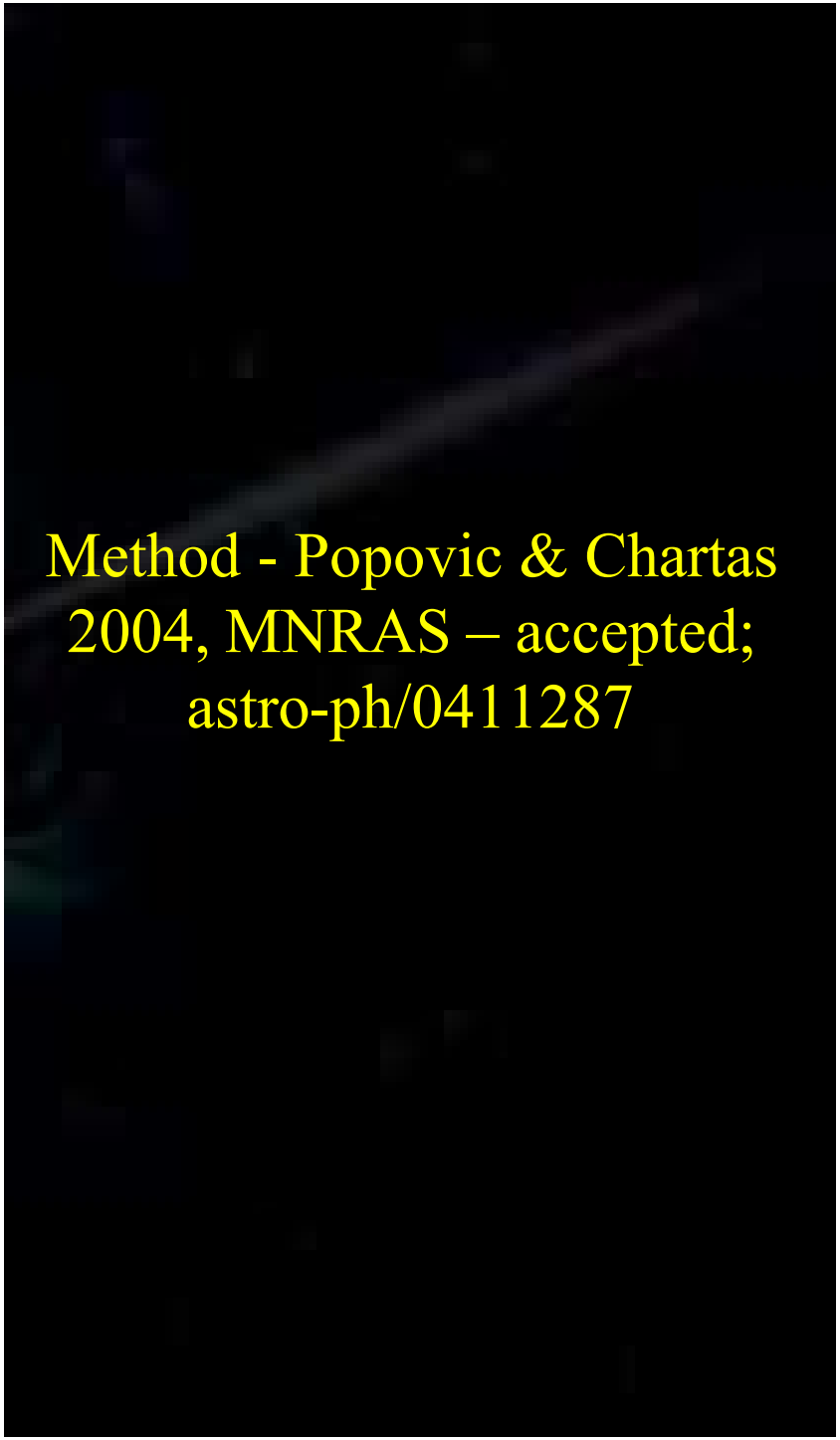

The 4 cases

Table 1. A list of cases where our proposed method can be used to infer the presence of millilensing, microlensing and intrinsic variability.

The case	Description
I) $\sigma = 0$ and $R_{AB} = R_{A'B'} = const.$	No variability or millilensing present
IIa) $\sigma = 0$, $R_{AB} = R_{A'B'} = f(\lambda)$ and/or $A^L \neq A^c$ IIb) $\sigma = 0$, $R_{AB} = R_{A'B'} = const.$ and $A^L \neq A^c$	There is no variability, but millilensing or differential extinction might be present (see e.g., Wucknitz et al. 2003), if $R_{AB} = f(\lambda)$ cannot be explained by extinction $\rightarrow$ millilensing is present
III) $\sigma \neq 0$, $\sigma_I \neq 0$, and $R_{A'B} = \frac{A_1}{A_2}$	Intrinsic variability is present
IVa) $\sigma \neq 0$, $\sigma_I = 0$, $R_{A,B} \neq f(\lambda)$ and $R_{A',B'} = f(\lambda)$	Microlensing of one image at time t_1
IVb) $\sigma \neq 0$, $\sigma_I = 0$, $R_{A,B} = f_1(\lambda)$, $R_{A',B'} = f_2(\lambda)$ and $R_{A'A} = 1$ (or $R_{B'B} = 1$)	Microlensing of one image at times t_0 and t_1 (timescale of microlensing is longer than time delay)

The case of Q0957+561: intrinsic variation seen on Jan 26 1995

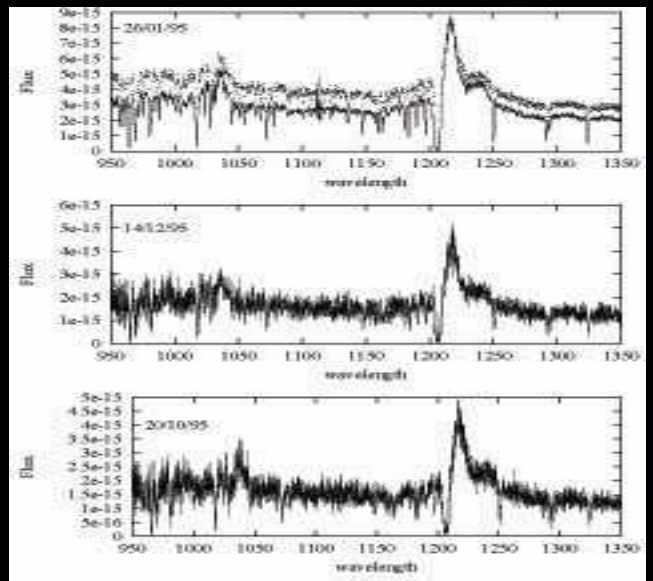

Figure 1. The spectra **(rest wavelength)** of Q0957+561 observed with HST for three different epochs. The solid line and dots indicate the spectra of images A and B, respectively. The flux is given in erg $cm^{-2}sec^{-1}A^{-1}$.

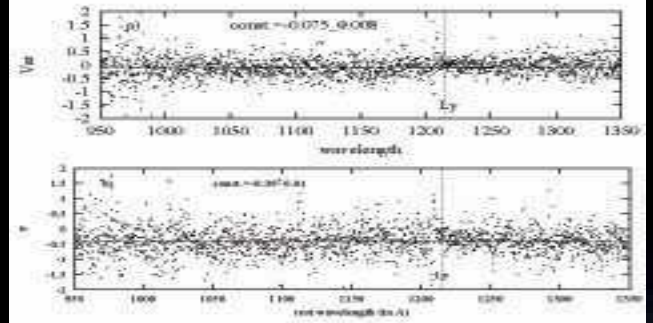

Figure 2. The variability indicator $Var = \sigma = (I'_A/I_A) - (I'_B/I_B)$ calculated for the spectra of Q0957+561 for the epochs: a) 1995 December 14 and 1995 October 20 (case I); b) 1995 January 26 and 1995 December 14 (case II). The vertical dashed line indicates the location of the Lyα line **(rest wavelength)**.

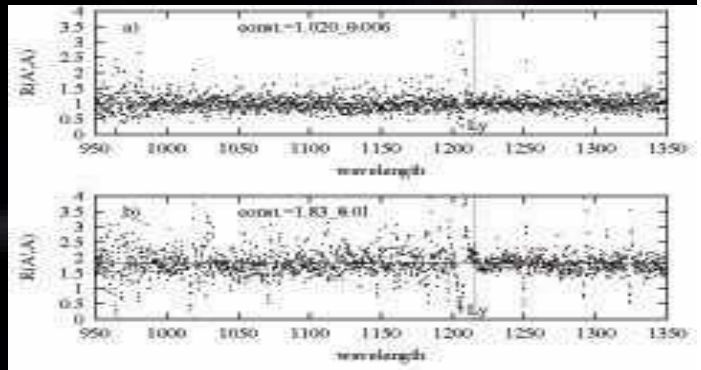

Figure 3. The flux ratio between the spectra of image A of Q0957+561 for the epochs: a) 1995 December 14 and 1995 October 20 (case I); b) 1995 January 26 and 1995 December 14 (case II). **The wavelength scale is givne in rest wavelength.**

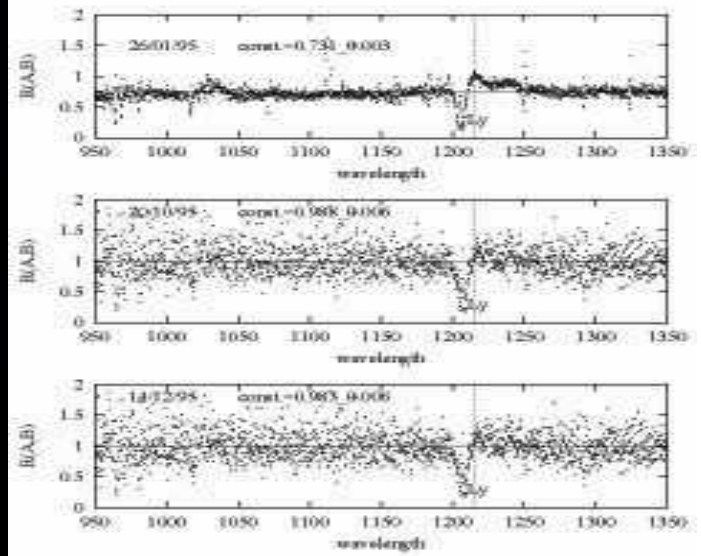

Figure 4. The flux ratio between images A and B of Q0957+561 observed for the listed epochs.

a) 1995; Oct. & Dec. b) 1995; Jan.& Dec.

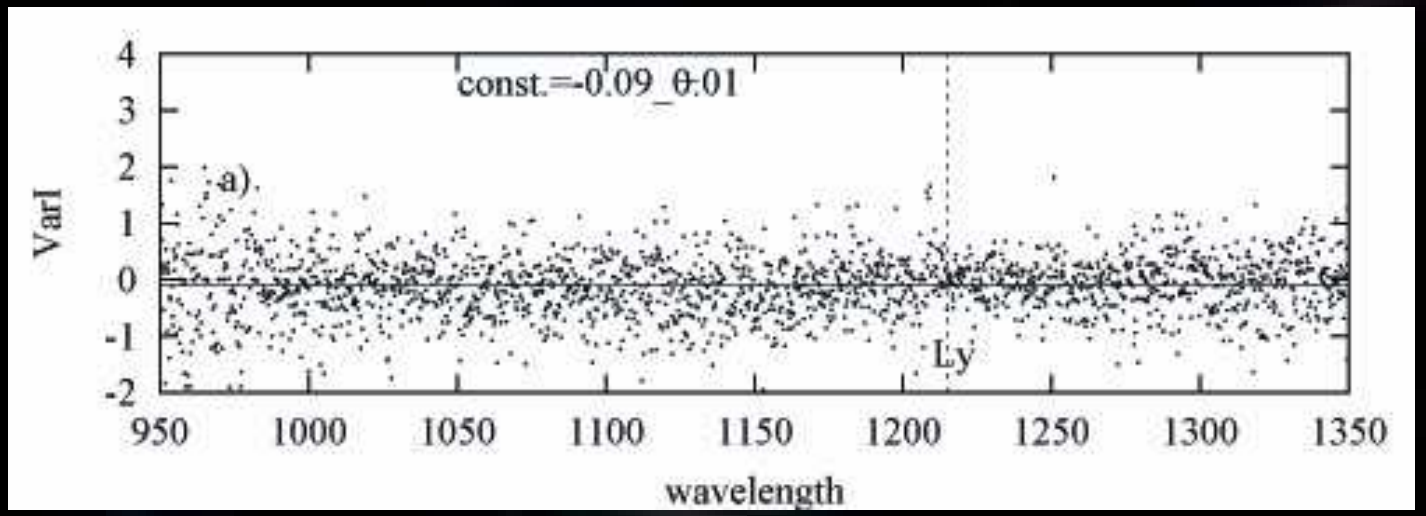

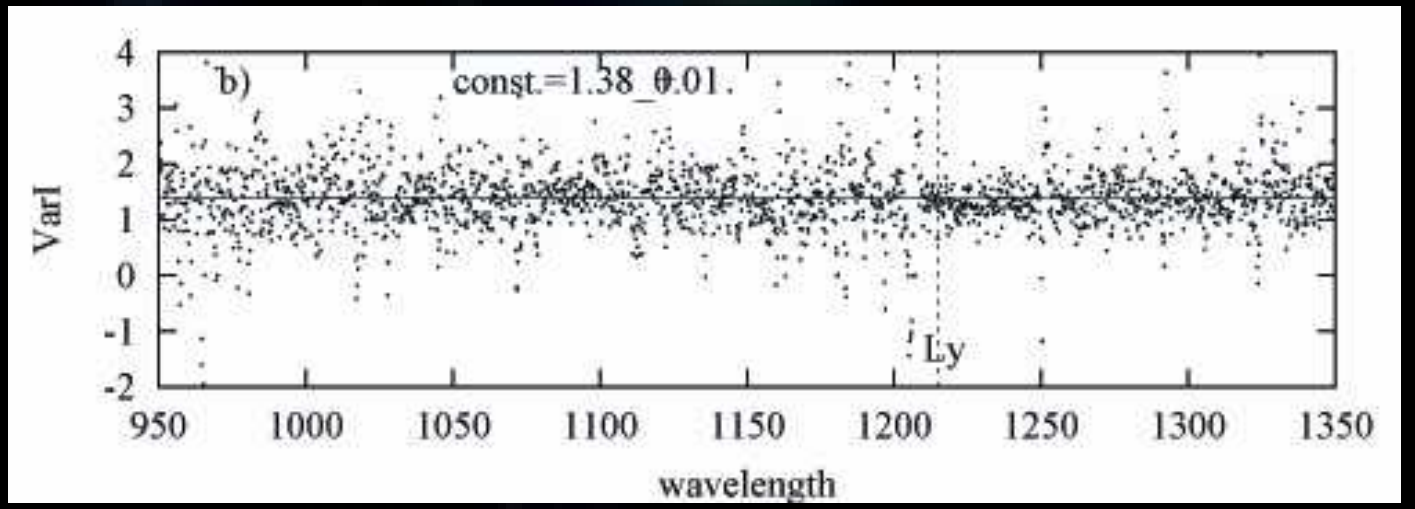

PG 1115+080 – probably millilensing, confirmed results of Impey et al. 1998; but long-term microlensing may produce a similar effect [Observations: 1995, July and 1996 January]

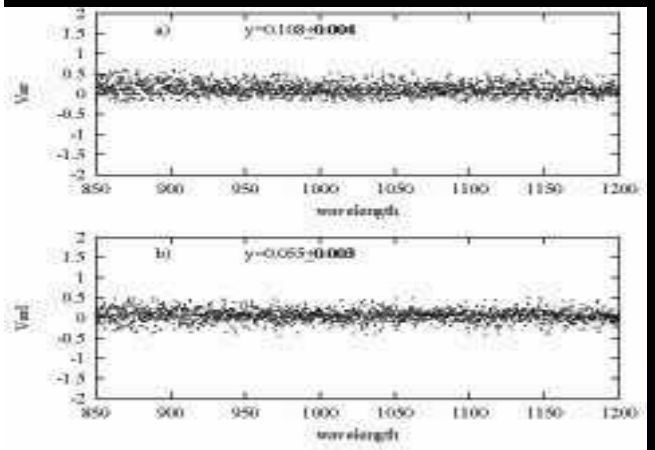

Figure 6. a) The variability indicator ($Var = \sigma$) and b) intristic variability indicator ($Var_I = \sigma_I$) between images A1 and A2 of PG 1115+080

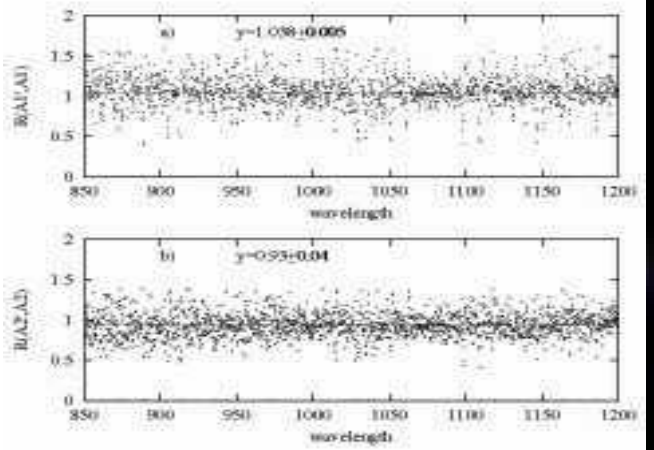

Figure 7. The flux ratio between epochs 1995 July and 1996 January for a) image A1, and b) image A2.

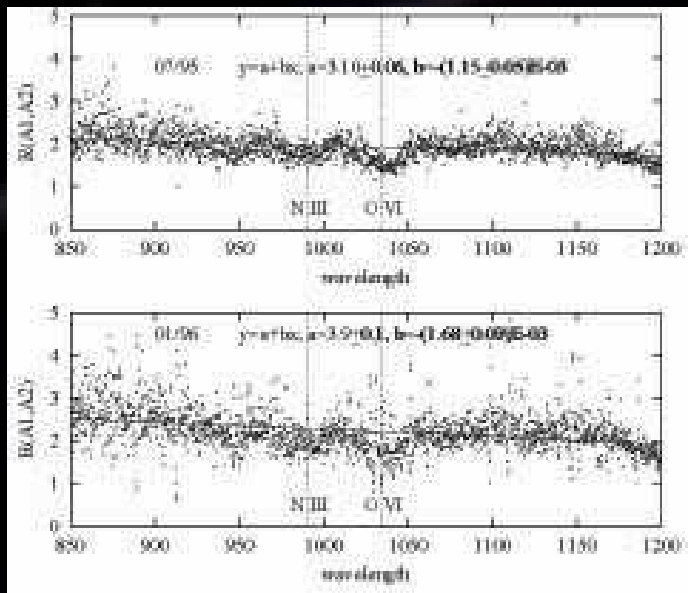

Figure 8. The flux ratio as a function of wavelength between images A1 and A2 of PG 1115+080 for two different epochs

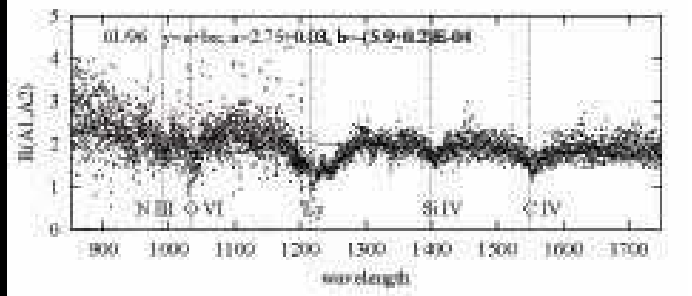

Figure 9. The flux ratio of images A1 and A2 of PG 1115+080 in the wavelength band of 850 – 1750 Å

What is with the UV line amplification?

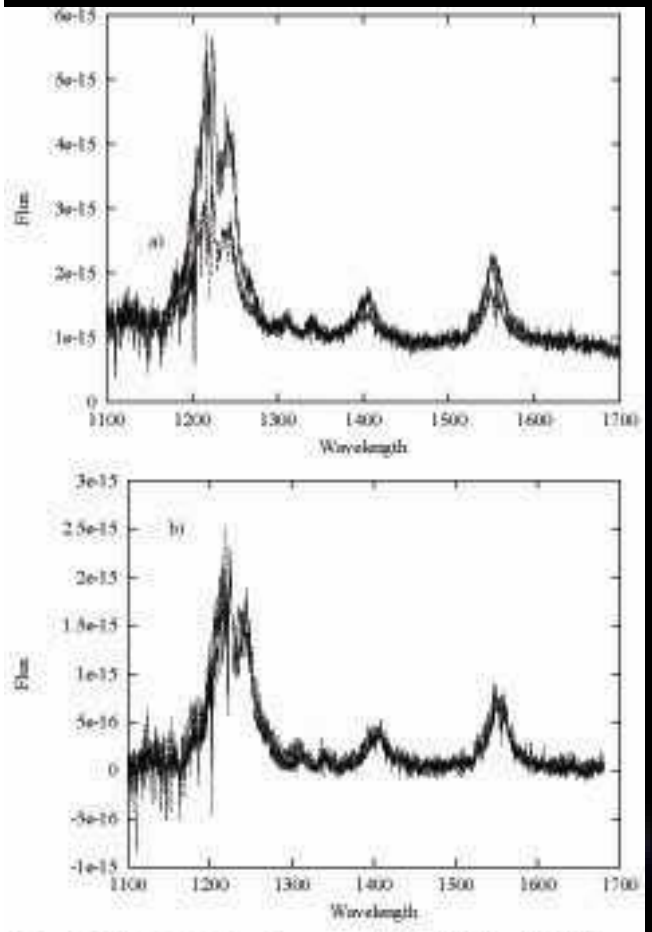

Figure 10. The flux (given in erg cm^{-2}sec^{-1}A^{-1} units) of image A1 of PG 1115+080 (dashed line) compared to that of image A2 of PG 1115+080 (solid line): a) after scaling the spectra of both images to the same continuum (the continuum level of image A1), and b) after subtraction of the continuum in both images.

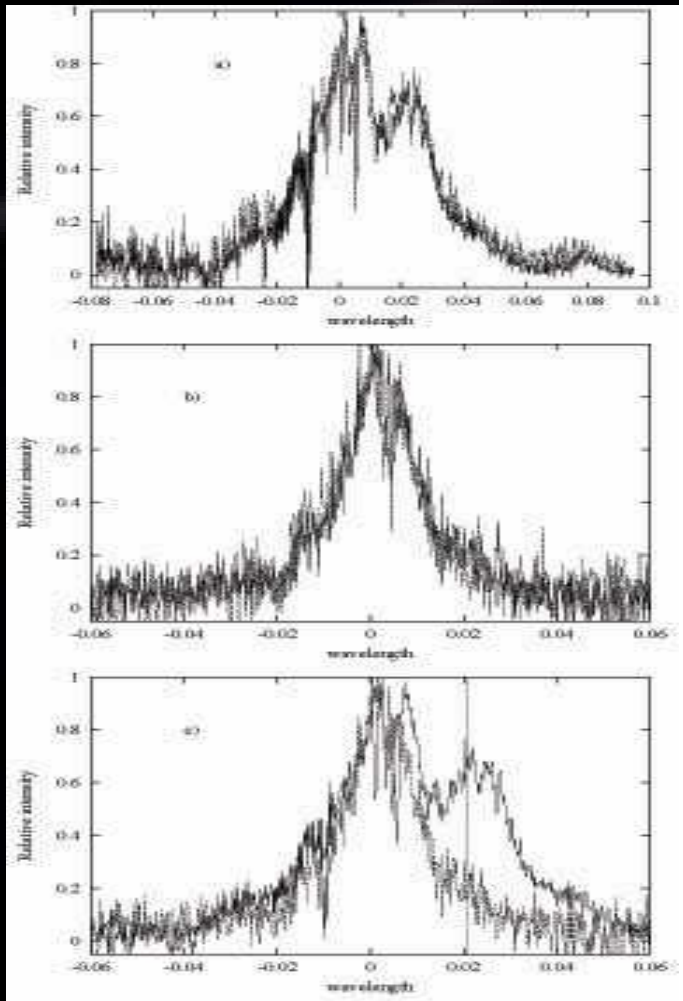

Figure 11. A comparison between : a) the Lyα line profiles of images A1 and A2 of PG 1115+080; b) the C IV line profiles of images A1 and A2 of PG 1115+080; c) the Lyα and C IV line profiles of image A2 of PG 1115+080 (the vertical dashed line shows the position of the N vA1240 line).

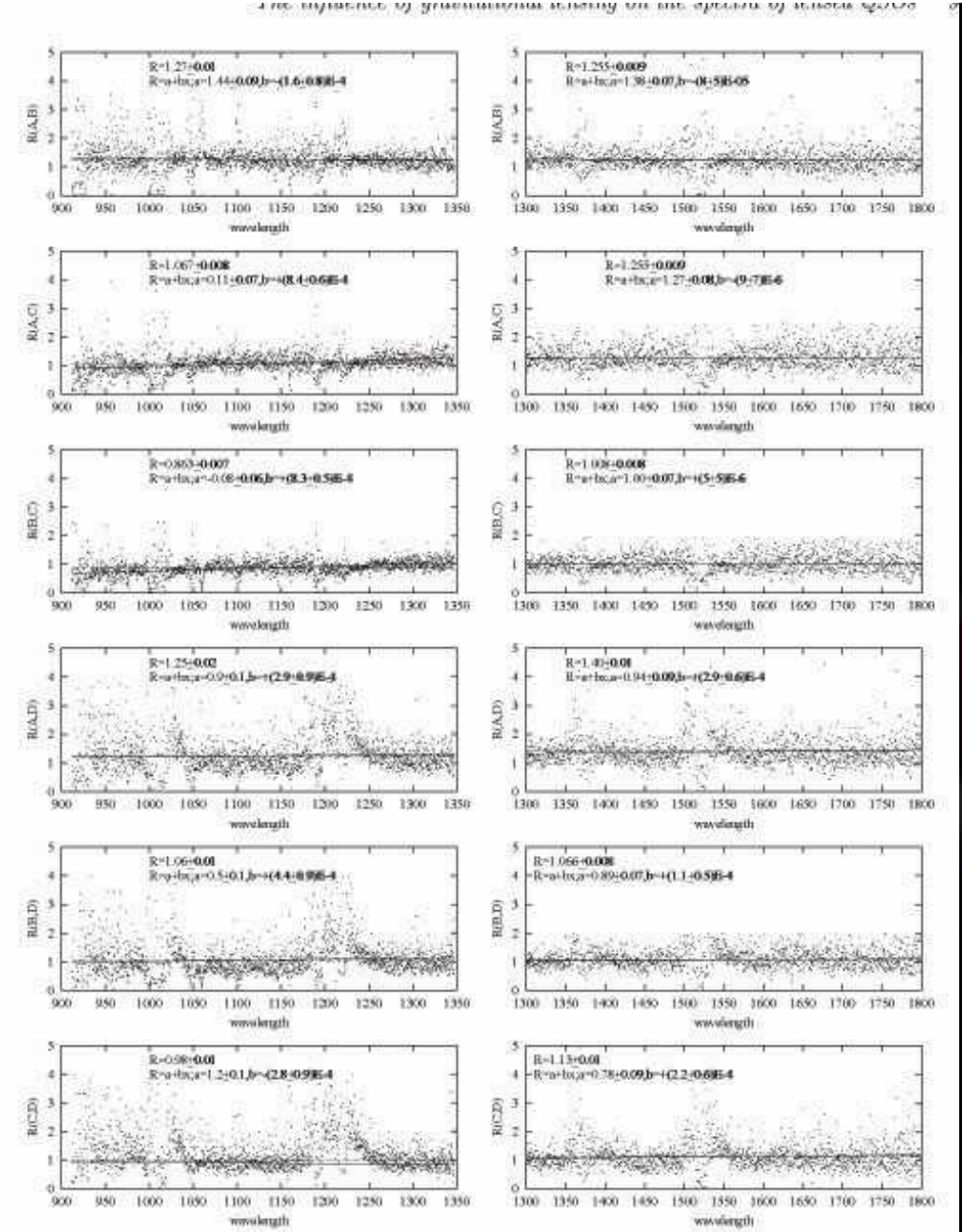

Figure 12. The flux ratio ($R_{i,j}$) of different images of QSO 1413+117 observed on the same date. Left panels: $R_{i,j}$ versus wavelength ranging from 900 Å to 1350 Å. Observations were made on 1994 December 24. Right panels: $R_{i,j}$ versus wavelength ranging from 1300 Å to 1800 Å. Observations of images A and D were performed on 1993 June 23 and of images B and C on 1993 June 27. From top to bottom, we show the flux ratios between the following images: A and B, A and C, B and C, A and D, B and D, C and D. The solid and dashed lines indicate the best fits of $R_{i,j} = a + b \cdot \lambda$ and $R_{i,j} = const$, respectively.

Q1413+117 – Cloverleaf : temporal variation in the continuum of image C – microlensing may be present during observations

Conclusions:

- Magnification may be chromatic (e.g. Wambsganss & Paczynski 1991)
- Influence of GL on QSOs spectra ➔ complex QSO emitting region geometry + complex potential of a lensing galaxy
- MLE ➔ wavelength dependent magnification
- The proposed method can infer the presence of microlensing, millilensing, and intrinsic variability
- OBSERVATIONS: from several periods (time delay = period between observations); 3D spectrophotormetry that can provide simultaneous spectra of all images